LA-UR- 00-796

Approved for public release; distribution is unlimited.

Title:	4D RECONSTRUCTIONS FROM LOW-COUNT SPECT DATA USING DEFORMABLE MODELS WITH SMOOTH INTERIOR INTENSITY VARIATIONS
Author(s):	Gregory S. Cunningham and Andre Lehovich
Submitted to:	Proceedings Medical Imaging 2000

Los Alamos
NATIONAL LABORATORY

Form 836 (10/96)

DISCLAIMER

4D reconstructions from low-count SPECT data using deformable models with smooth interior intensity variations

Gregory S. Cunningham[a] and Andre Lehovich[b*]

[a] Los Alamos National Laboratory, MS P940, Los Alamos, NM
[b] University of Arizona, Dept. of Applied Mathematics, Tucson, AZ

ABSTRACT

The Bayes Inference Engine (BIE) has been used to perform a 4D reconstruction of a first-pass radiotracer bolus distribution inside a CardioWest Total Artificial Heart, imaged with the University of Arizona's FastSPECT system. The BIE estimates parameter values that define the 3D model of the radiotracer distribution at each of 41 times spanning about two seconds. The 3D models have two components: a closed surface, composed of bi-quadratic Bezier triangular surface patches, that defines the interface between the part of the blood pool that contains radiotracer and the part that contains no radiotracer, and smooth voxel-to-voxel variations in intensity within the closed surface. Ideally, the surface estimates the ventricular wall location where the bolus is infused throughout the part of the blood pool contained by the right ventricle. The voxel-to-voxel variations are needed to model an inhomogenously-mixed bolus. Maximum a posterior (MAP) estimates of the Bezier control points and voxel values are obtained for each time frame. We show new reconstructions using the Bezier surface models, and discuss estimates of ventricular volume as a function of time, ejection fraction, and wall motion. The computation time for our reconstruction process, which directly estimates complex 3D model parameters from the raw data, is performed in a time that is competitive with more traditional voxel-based methods (ML-EM, e.g.).

Keywords: Bayesian inference, deformable models, Bezier patches, 4D reconstruction, dynamic cardiac SPECT

1. INTRODUCTION

The FASTSPECT imaging system[1], developed at the University of Arizona, has been used for first-pass tomographic imaging of the time-varying distribution of a bolus of Tc-99m pertechnetate radiotracer infused into a CardioWest Total Artificial Heart. The FASTSPECT machine simultaneously provides 24 pinhole views of the bolus distribution evolving in time, and is unique in its ability to perform this type of dynamic imaging. The goal in obtaining first-pass tomographic data is to demonstrate that clinically important measures of heart function, such as ejection fraction and wall motion, can be quantitatively estimated without having to gate and average over many cardiac cycles, an approach necessarily utilized by single- or dual-head cardiac SPECT systems. If ejection fraction and wall motion can be estimated from first-pass data during the first few cardiac cycles, then later cycles can be used to estimate myocardial perfusion, another important indicator of heart function. If successful, the FASTSPECT approach would mean that a single, relatively cheap instrument could perform multiple diagnostic tests of cardiac function with a single bolus of radiotracer. This type of capability would be clinically valuable and affordable for use in emergency rooms across the country to do initial assessment of cardiac patients.

In order for the first-pass data to provide information on ejection fraction and wall motion, the tracer must be observed in a state in which it is distributed throughout the blood pool contained by the ventricle, so that the physical extent of the bolus is coincident with the walls of the ventricle wherever the ventricular walls are present. If this assumption is valid, then one might simply reconstruct the intensity of the bolus, perform segmentation on the results, and post-process to identify the location of the ventricular wall as a function of time. This "reconstruct and segment" approach has been used in other medical imaging modalities. However, for FASTSPECT's low SNR environment, with very few tomographic views, the estimate of the ventricular wall that would result from such an approach is sub-optimal. An alternative approach, adopted here, is to model the distribution of tracer as a surface, inside of which the tracer intensity varies smoothly. Then, under the further assumption that this model correctly describes the true distribution of tracer at a given time, one can find a better estimate of the ventricular walls at that time by directly estimating the parameters of the surface from the raw data. One might assume that the "direct estimation" approach is more computationally intensive and more difficult to automate than the

* Further author information: (Send correspondence to G.S.C.)
G.S.C.: E-mail: cunning@lanl.gov
A.L.: E-mail: lehovich@math.arizona.edu

"reconstruct and segment" approach; however, we have found that our implementation of the direct estimation approach is computationally competitive with the traditional approach and is amenable to automation.

Others have attempted to directly estimate 2D and 3D shape parameters from various sorts of tomographic data; however, we were the first to directly estimate 3D triangulated surface models from SPECT data. In our initial work, we assumed that either a "smooth" 2D closed contour[2] or 3D closed surface[3], with a constant interior intensity, was an adequate model for the tracer distribution at a given time. We found that inhomogeneities in tracer intensity were the probable cause of artifacts we observed in our first analysis of real data, and soon after we introduced smooth variations in intensity within the closed surface in order to accommodate the inhomogeneity[4]. Our earlier work also assumed that the smallest surface that encloses the tracer can be adequately modelled as a "smooth" one, but when the bolus is transported through the inlet tube into the right ventricle, and then out of the ventricle into the outlet tube, the smallest surface that contains all of the tracer must have very high-frequency features at the tube/ventricle join. In our current work, we relax the smoothness assumption in the tube/ventricle join areas, as defined by user placement of a 5 cm diameter sphere, an idea we discussed earlier in the context of 2D models[5].

In our earlier work, we found it difficult to automate the direct estimation due to the large number of nonlinear relationships between the vertices that parameterize the surface model and the predicted detector count rates implied by the parameterized distributions of tracer. We observed significant "mesh-tangling" during the optimization process, and the user had to frequently refine and remesh the surface as it was being optimized[6,7]. In our current work, we use bi-quadratic Bezier triangular surface patches[8] to better control the surface shape during optimization. When one time frame has been analyzed, the surface is automatically refined (by splitting all patches whose shared edges have an arclength that exceeds about 5 mm) before analysis on the next time frame is started. The fewer number of higher-order patches means that the mesh refinement is easy to automate without creating mesh connectivity problems.

The two incremental improvements we have made in our approach to this data (user-labelled regions of high-frequency surface kinks and Bezier surface patches) now allow us to automatically extract quantitative estimates of the surface and interior intensity variations for a whole sequence of time frames without user intervention. The compute time is about 4 minutes per frame on a DEC 500/500 (500 MB memory, 500 MHz CPU), competitive with the reconstruction-only part of a reconstruct and segment approach. We use the automated capability to produce quantitative estimates of ventricular volume as a function of time, ejection fraction and wall motion. We find that, due primarily to the tracer inhomogeneity, the surface estimate is not coincident with the ventricular wall in all regions. However, an appropriate threshold can be chosen so that the segmentation of the volumetric reconstruction using this threshold produces the correct minimum volume and ejection fraction for the artificial heart (to within a few percent). These results are superior to those obtained for our implementation of ML-EM, where the best threshold one can find produces volume estimates that are in error by about 30%. Also, in regions where the surface is coincident with the iso-intensity contour at the optimal threshold, we have good reason to believe that the surface indeed is coincident with the ventricular wall and can be used to measure wall motion.

The rest of the article is organized as follows: first we give a brief overview of FASTSPECT and the data we analyzed. Next, we formulate the Bayesian estimation problem that provides the foundation for direct estimation from the raw data. We show results on ventricular volume, ejection fraction and wall motion, and compare these results with those obtained using ML-EM. Finally, we draw some conclusions and discuss possible future directions.

2. THE DATA

2.1. FASTSPECT

FASTSPECT is a dynamic SPECT imager that has been used for brain, heart and bone imaging[1]. Two circular arrays with a total of 24 pinhole apertures are arranged on a hemispherical dome that is roughly 35 cm in diameter. The hemisphere surrounds the volume of interest. Each pinhole is mapped to an Anger detector, and an estimate of the position of each detected photon must lie on a 64x64 uniformly-binned image grid. If a reliable estimate of the position of a photon cannot be determined, then the photon hit is discarded. Pinholes of various diameter can be inserted into the dome surrounding the object volume; 4.0 mm diameter pinholes were used to generate the data analyzed in this article. The system is characterized by a matrix, **H**, that is measured by passing a small volume element of radiotracer throughout the volume being imaged, and measuring the response of every detector pixel to that source. This produces an enormous amount of information, even when compressed to take advantage of the sparsity of the matrix (150 MB of disk space after compression; 300 MB after partial uncompression in memory to speed up the calculation). The system matrix used in this article was obtained by passing a $[5\text{mm}]^3$ volume element through a 43x57x39 grid. The system matrix is noisy, since only a finite number of counts are

obtained for each location of the source. Given enough patience and time, though, this noise could presumably be made as low as is needed. Note that attenuation through the dome is included in the measurement of **H**. If information is available concerning attenuating material between the radiotracer distribution and the pinholes, it can also be incorporated into **H**, and this was done for the **H** used to analyze the data discussed in this article[3].

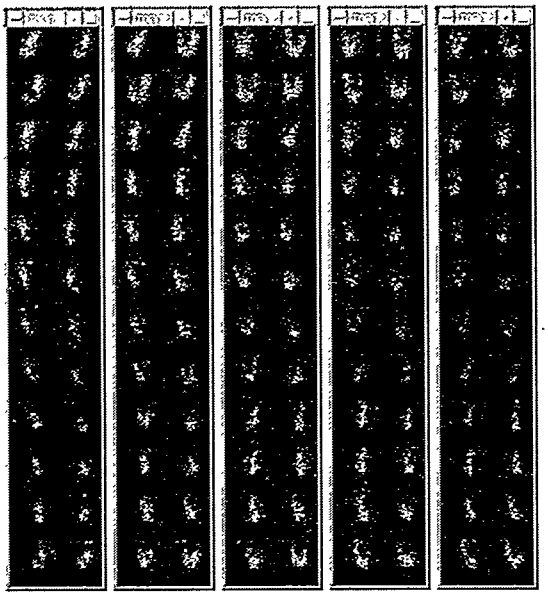

a) b) c) d) e)

Figure 1. Raw data for frames a) 46 b) 56 c) 66 d) 76 and e) 86.

2.2. The imaged object and raw data

The object that was imaged is a CardioWest Total Artificial Heart. Only the left and right ventricles, each about 120 ml in volume, were used. The lungs were simulated using bottles filled with water and styrofoam beads. A 20 mCi bolus of Tc-99m pertechnetate was injected into the input tube of the right ventricle at a site outside the field of view about 17 cm from the input valve of the right ventricle. The 20 mCi is first placed into 0.5 mL of a syringe and injected into a very small tube that leads to the input tube of the right ventricle. The bolus is eventually "flushed" into the input tube using a volume of water that is greater than the volume enclosed by the small tube. This process is thought to parallel the method of injection for humans, in which the injection is followed by a saline flush. Ultimately, the fluid flows into and out of a Donovan mock circulatory system, which is out of the field of view.

We present analysis results for 41 of the 150 50-msec frames that were available (frames 46-86) during which time the bolus just starts to enter the right ventricle from the input tube, mixes into the blood pool in the ventricle, and gets pushed out the output tube. Frame 46 (Figure 1a) contained a total of 4935 counts, of which a few percent appear to be inconsistent with the assumption that the radiotracer distribution is contained within the right ventricle and its associated input and output tubes. We assume that these counts are from photons that were scattered but still accepted, although other explanations may be possible. We refer to these counts as "background" counts, and will model and estimate this background as a single constant, different in value for each time frame, but the same for all detector pixels at a given time.

3. THE BAYESIAN ESTIMATION PROBLEM

We have implemented a general tool for Bayesian estimation, in the context of image analysis using geometric models, that we call the Bayes Inference Engine (BIE)[9]. We break the Bayesian estimation problem into three parts: the object model, the measurement model, and the probability model. In the BIE, the user constructs a graphical program that transforms object and measurement system parameters into predicted data. The predicted data are compared with real data to produce a minus-log-likelihood function, which is combined with prior information, to produce a minus-log-posterior. The minus-log-posterior is minimized as a function of the parameters that are to be estimated. See Figure 2 for the graphical program that was used to analyze the data discussed in this article.

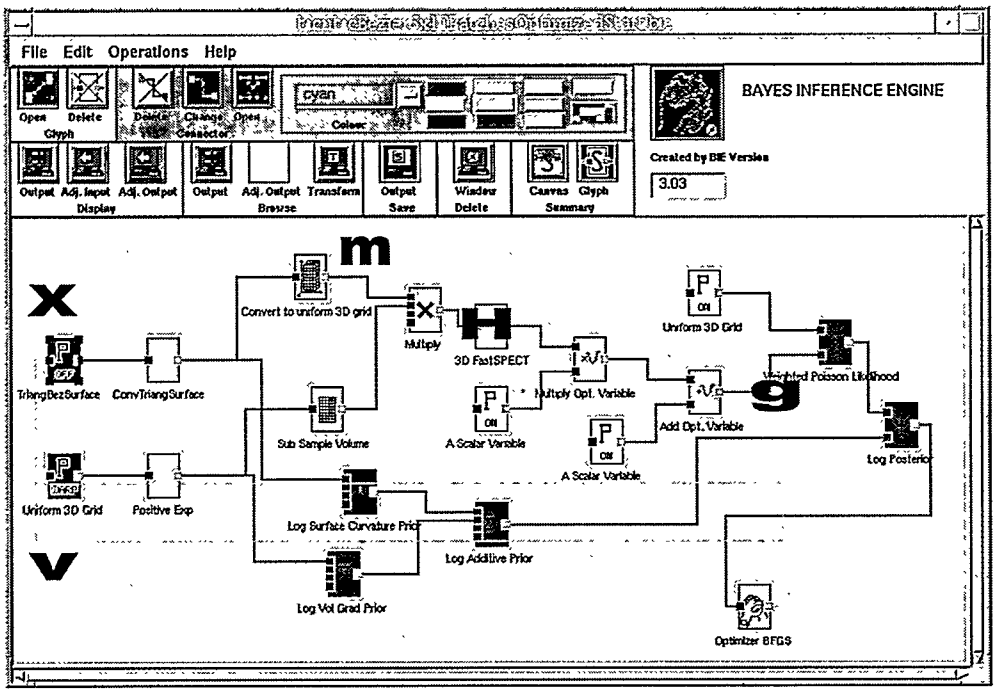

Figure 2. BIE canvas used to analyze FASTSPECT data. The upper left box (TriangBezSurface) contains the ~200-patch, bi-quadratic Bezier surface, **x**, which contains ~1200 control points. The lower left box (UniformGrid3D) contains the voxellated model, **v**, of dimensions 35x34x16. The Bezier surface is transformed first into a triangulated surface with ~1800 triangles (upper path), and ultimately into a voxellated grid to produce a (mostly binary) mask, **m**, that is multiplied by the embedded volume model, Embed(exp(**v**)), to produce, **f**, the final voxellated grid model for the tracer distribution. **f** is multiplied by the matrix, **H**, to produce **Hf(x,v)**. Finally the normalizer, I, is applied and the additive background constant, s, is added, to produce the predicted detector pixel rates **g=IHf(x,v)**+s. The exp(v) transform is used to insure positivity of the estimate for **v** without resorting to inequality constraints.

3.1. The object model

The object model in this case is the parametric model for the 3D radiotracer intensity distribution. In the BIE, we always convert parametric models to non-parametric ones (uniformly sampled grids) so that complex models can easily be built through combination of parametric models after conversion to a non-parametric form. The parameteric model for the minimal surface that contains the tracer is a set of ~200 bi-quadratic triangular Bezier patches, each patch specified by a set of 6 control points, along with a connectivity network that creates the surface by connecting patches together (Figure 3a). The ~3600-point vector that lists the (x,y,z) components for each of the ~1200 control points is denoted **x**. This parametric model is converted to a non-parametric uniformly-voxellated grid by first converting the Bezier-patched surface into a triangulated surface (each Bezier patch is converted into a 9-triangle surface patch (Figure 3b)). Next, the triangular surface patches are sown together using the connectivity network of the Bezier-patched surface, and the resulting closed triangulated surface is converted to a non-parametric uniformly-voxellated grid by setting the value of each voxel in **m** to the fraction of that voxel that is contained within the volume described by the triangulated surface[6,7]. The mask **m** is multiplied by the embedded voxellated grid, Embed(exp(**v**)), so that the final tracer distribution model, **f=m(x)***Embed(exp(**v**)), allows for smooth voxel-to-voxel variations within the closed surface and rapid transitions in intensity across the surface boundary. **f** must have the proper dimensions in order to be operated on by the system matrix, **H**, which is the reason for the Embed(*) operation (**v** has the minimal number of parameters needed for a rectangular volume to cover the region of non-zero intensity). The exp(**v**) transform is used to insure that the estimate for v is positive. We have found that this reparameterization produces better results in the context of the BIE's BFGS optimizer than explicit enforcement of non-negativity constraints on the values in **v**.

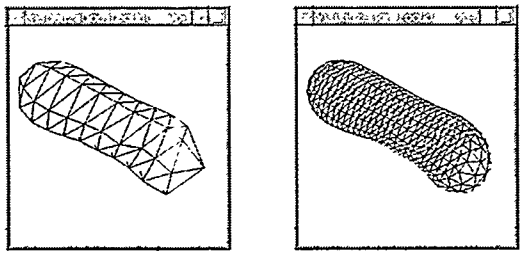

a) b)

Figure 3. The initial configuration of the Bezier surface model for frame 46 (front part of surface only, back part is clipped). Each bi-quadratic patch is sampled with a) 1 triangle and b) 9 triangles.

3.2. The measurement model

The measurement model uses as input the nonparametric version of the object model, **f**, and produces a set of predicted data elements, **g**, in this case a Poisson rate for each detector pixel. For the FASTSPECT machine, the measurement model is merely the system matrix, **H**, along with a single additive constant that models the background (the same background constant is used for all 24 detectors), so that **g=IHf+s**. The constant, I, is used to normalize the solution so that the voxel values, **v**, are nominally 1.0 for the first analyzed frame, if no intensity variation is required. The background, **s**, must be jointly estimated from the data along with the object model parameters. The nature of our object model allows us to speed up the calculation **Hf** dramatically since only a few percent of the voxels in **f** are nonzero. Simply skipping over the calculation **Hf** for values of **f** that are zero allows us to calculate **Hf** in about 300 msec on a DEC Alpha 500/500. The same speedup applies in the adjoint direction, wherein derivatives of the minus-log-posterior are propagated according to the chain rule in the direction opposite to the path that transforms object parameters into predicted data[9]. At the end of the adjoint calculation, the derivatives of the minus-log-posterior wrt object parameters are obtained. These derivatives take about the same compute time to produce as does one forward calculation of the predicted data, starting from the object parameters. One pair of forward-adjoint calculations is needed for each iteration of the BFGS optimization algorithm, which is used to find the MAP solution (see section 3.4), and takes 5-6 seconds to produce. Since 40 iterations of BFGS are used to find the MAP solution, each frame takes approximately 4 minutes to process, yielding a 41-frame reconstruction in about 2½ hours on this machine. The adjoint calculation, the small region of non-zero support associated with the surface model, and the availability of the system matrix **H**, are the reasons why our implementation of the direct estimation approach is computationally competitive with a traditional approach like ML-EM.

3.3. The probability model

The prior probability model for the surface, **x**, is indirect. First, the Bezier surface is converted to a triangulated surface with 9 triangles per Bezier patch, as in section 3.1. The prior penalizes a discrete approximation to the local curvature at every edge shared by two triangles on the triangulated surface in order to enforce smoothness of the estimated surface[3]. Let $\mathbf{n}_i$ be the normal to the i^{th} triangle. We define θ_{ij} to be the angle between $\mathbf{n}_i$ and $\mathbf{n}_j$. Then, if A_i is the area of the i^{th} triangle, and l_{ij} is 1/3 the height of the i^{th} triangle relative to the edge shared by triangles i and j, the curvature prior is defined as

$$\pi_{\text{surf}}(y) = \sum_i A_i \sum_j \left(\frac{\tan(\theta_{ij}/2)}{l_{ij}} \right)^2, \tag{1}$$

where **y** is the list of (x,y,z) components for all of the vertices, i indexes over all triangles on the triangulated surface and j indexes over all triangles that share an edge with the i^{th} triangle.

The prior probability model for the volume, **v**, penalizes the voxel-to-voxel variations in intensity in order to make inhomogeneities in the tracer distribution within the closed surface smooth:

$$\pi_{\text{volume}}(v) = \sum_{ijk} \left\| \nabla v_{ijk} \right\|^2 \tag{2}$$

where

$$\nabla v_{ijk} = \begin{pmatrix} (v_{i+1,j,k} - v_{i,j,k}) \text{ if } 1 \le i \le N_x; 0 \text{ else} \\ (v_{i,j+1,k} - v_{i,j,k}) \text{ if } 1 \le j \le N_y; 0 \text{ else} \\ (v_{i,j,k+1} - v_{i,j,k}) \text{ if } 1 \le k \le N_z; 0 \text{ else} \end{pmatrix}$$

and N_x=35, N_y=34, and N_z=16.

The probability model for the likelihood is the Poisson distribution with mean value equal to the predicted data (predicted detector pixel Poisson rates, $\mathbf{g}=\mathbf{I}\mathbf{H}\mathbf{f}(\mathbf{x},\mathbf{v})+\mathbf{s}$) and count values equal to the actual detector counts, $\mathbf{k}$:

$$\begin{aligned} \phi(\mathbf{x},\mathbf{v},\mathbf{I},\mathbf{s}) &= -\ln \text{Prob}[\text{data} \mid \text{predicted data}] \\ &= \Sigma_i [-k_i \ln g_i + g_i] + C(k), \end{aligned} \tag{3}$$

where $C(\mathbf{k})$ has terms that depend only on $\mathbf{k}$. The dependence of the predicted data $\mathbf{g}$ on the underlying parameters $\mathbf{x}$, $\mathbf{v}$, I, and s, is understood.

3.4. The estimation problem

The Bayesian estimation problem is to find the values for the object model parameters, $\mathbf{x}$, $\mathbf{v}$, that produce the maximum *a posteriori* (MAP) probability, or the minimum minus-log posterior:

$$(\mathbf{x}^{MAP}(\alpha,\beta), \mathbf{v}^{MAP}(\alpha,\beta)) = \arg\min_{x,v} [\phi(\mathbf{x},\mathbf{v},\mathbf{I},\mathbf{s}) + \alpha\pi_{surf}(\mathbf{x}) + \beta\pi_{volume}(\mathbf{v})], \tag{4}$$

for some fixed values of the hyperparameters, α, β. The higher-order problem is to determine the values of α, β, from the data. A Bayesian solution to the higher-order problem that we have used in the past is to select the hyperparameters that yield the greatest evidence for the data, where the evidence is the integral w.r.t. parameters over the joint posterior distribution of parameters and data (leaving just the probability of the data given the hyperparameters, called the evidence)[4]:

$$(\alpha,\beta)_{ML} = \arg\max_{(\alpha,\beta)} \text{Evidence}(\alpha,\beta)$$

In our past work, we demonstrated the use of an algorithm to compute the evidence, but the algorithm was very difficult to implement for our problem. We found that the best values for the hyperparameters vary significantly for different time frames, due to the fact that the bolus has to make two "right turns" to get into the ventricle from the input tube, and then out of the ventricle again and into the output tube. These high-curvature turns mean that at later times, weaker surface priors are demanded by the data, while at earlier times there is no evidence for distinguishing between two good solutions: a weak surface prior combined with a strong volume prior, or a strong surface prior with a weak volume prior. In both early and late time frames, there is evidence in the data of significant inhomogeneities in tracer intensity, and thus a relatively weak volume prior is required.

Our previous work was done without allowing "kinks"[5] to develop at the tube/ventricle joins. In order to allow the bolus to make the two "right turns" while still maintaining a strong surface prior elsewhere, we deweight the surface prior in a user-defined region. The user positions a sphere of diameter 5 cm (equal to ten voxel widths), centered at the two tube/ventricle joins (Figure 4), which can be roughly obtained from a poorer-quality initial reconstruction of a single time frame (e.g. ML-EM). If the vertex of any edge of the triangulated surface is inside this sphere, then the contribution to the surface prior from that edge is set to zero. Thus, high-frequency kinks are allowed to develop across edges that have at least one vertex in this sphere. Figure 5 contains a visualization of the improved ability of the surface to properly contain the bolus distribution, while better matching the expected geometry at the tube/ventricle joins, using deweighting of the prior. The deweighting of the prior may change the shape of the evidence as a function of the hyperparameters, but we have not explored computing the evidence with the deweighted prior. For early time frames, deweighting of the prior does not appear to influence the MAP solution, and so we would expect the evidence to be similarly unaffected.

Since the evidence is costly to compute, we make the argument that the optimal value of the hyperparameters will not be too different for different time frames using the deweighted prior, and so we need to compute the optimal values only for the first frame (46), which we discussed in previous work[4]. The optimal values of the hyperparameters obtained for this frame are then used for all subsequent time frames. We use α=3.16, β=0.56, for all of the estimates of ventricular volume, ejection fraction, and wall motion discussed in Section 4.

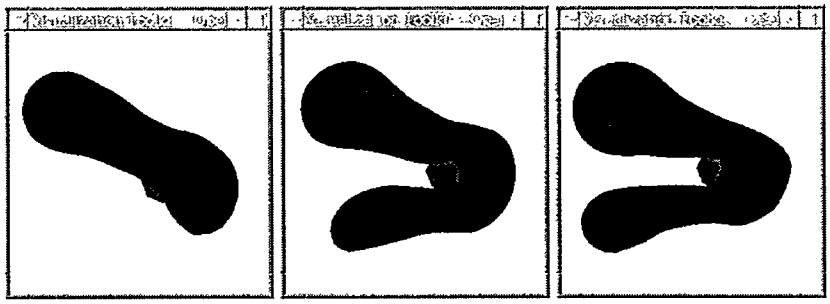

a) b) c)

Figure 4. MAP estimates of surface for frames a) 46, b) 56 and c) 76 using α=0.5, β=2.0 (weak surface prior, strong volume prior). The user-positioned sphere (light gray) between the input tube (top) and output tube (bottom) indicates the region where the surface smoothness prior is deweighted to allow surface "kinks" to form.

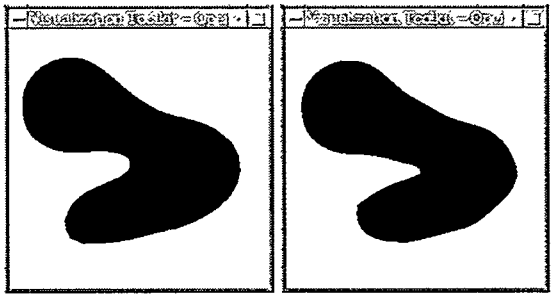

a) b)

Figure 5. MAP estimates of surface for frame 56 with α=1.0, β=1.0 (medium surface prior, medium volume prior) with a) no deweighting of prior and b) deweighting of prior as in Figure 4. The strong surface prior is encouraging a region of the surface to "grow between" the two tubes in a) in order to minimize the surface curvature.

3.5 Obtaining the MAP solutions for 41 time frames with minimal user intervention

With the incremental improvements discussed in the previous subsections (surface kinks and bezier patches) we are able to automatically extract the surface and volume estimates from the raw data once an initial surface model is in place. In addition, if the user specifies a sphere that a) grossly contains the ventricular volume, and b) separates the ventricular volume from the inlet and outlet tubes, then the surface estimates can be used to generate estimates of ventricular volume as a function of time, and ultimately ejection fraction.

The user must specify an initial geometrical model to be fitted to the raw data for the first time frame to be analyzed, in order to get the gross geometrical shape correct. We used a cylinder with constant interior intensity to match frame 46, where the radius, height, two spherical angles, and centroid are fitted by the BIE starting from user-inputted initial values for the cylinder that are coarsely correct. A handful of iterations of gradient-descent and conjugate gradient are used to obtain a fit to frame 46 for the intensity, I, and background, s, using the cylindrical model. The cylinder is then converted into a Bezier-patched surface using 6 discrete values in r and 10 discrete values in z to define a total of 120 patches. A few more iterations of gradient descent and conjugate gradient are used to produce a more reasonable fit to the surface, $\mathbf{x}$, and volume, $\mathbf{v}$. This is the point at which the user input ceases, and the time frames are fit automatically. The intensity, I, is not optimized anymore, as this is just a gross scaling factor that is intended to make the values in $\mathbf{v}$ close to 1 in the initial frame. The background, s, is obtained for future frames simply by scaling the overall counts relative to the total number of counts in the first frame (assumption is that the unscattered/background ratio is constant for all time frames).

The MAP estimates for $\mathbf{x}$ and $\mathbf{v}$ are produced for each time frame using BFGS to minimize the minus-log-posterior, with the values for the hyperparameters that were found to be optimal for frame 46. The initial configuration for each time frame is the MAP solution for the previous time frame, after remeshing by breaking all pairs of patches into four new patches if the shared edge has a total arclength greater than ~5mm. The initial inverse Hessian, required by the BFGS algorithm, is block-

diagonal, where the block that corresponds to x is set to (0.03/α)*I, and the block that corresponds to v is set to (28/β)*I. The constants were determined by inspection of the eigenvalues of the Hessians for the minus-log-priors and minus-log-likelihood, which are available as a byproduct of the evidence calculation for frame 46[4]. 40 iterations of BFGS were run for each time frame, which takes about 4 minutes on a DEC 500/500 (500 MB, 500 MHz), so that the 41 time frames were produced in about 2½ hours. We have recently purchased a quad-processor PC with 2 GB of shared memory for about $15,000, which we anticipate will shorten the compute time by about a factor of 4 once the code is multi-threaded to take advantage of the additional resources.

4. RESULTS

4.1. 4D reconstructions

A cursory examination of key frames in the 41-frame reconstructions (Figure 6) indicates evidence for significant inhomogeneity in the tracer intensity distribution that appears to move through the volume as time progresses. For a weak surface prior and strong volume prior (Figure 6 f-j), the surface estimate matches the 0.425 isocontour in the area of the ventricular wall, while for a strong surface prior and weak volume prior (Figure 6 a-e), the surface estimate is considerably larger than the 0.425 isocontour in the ventricular region, and large regions of the ventricular volume are essentially unconstrained by the surface model. This is discouraging news, since our goal was to use the surface to estimate the ventricular volume as a function of time and wall. In fact, even if we modify the goal to be "improve the quantitative accuracy of the reconstructions", one might ask "are we doing any better than ML-EM?". Fortunately, the answer to this last question at least appears to be "yes", although the high degree of inhomogeneity means the improvement over ML-EM, and the utility of the surface model, is not as much as we had hoped.

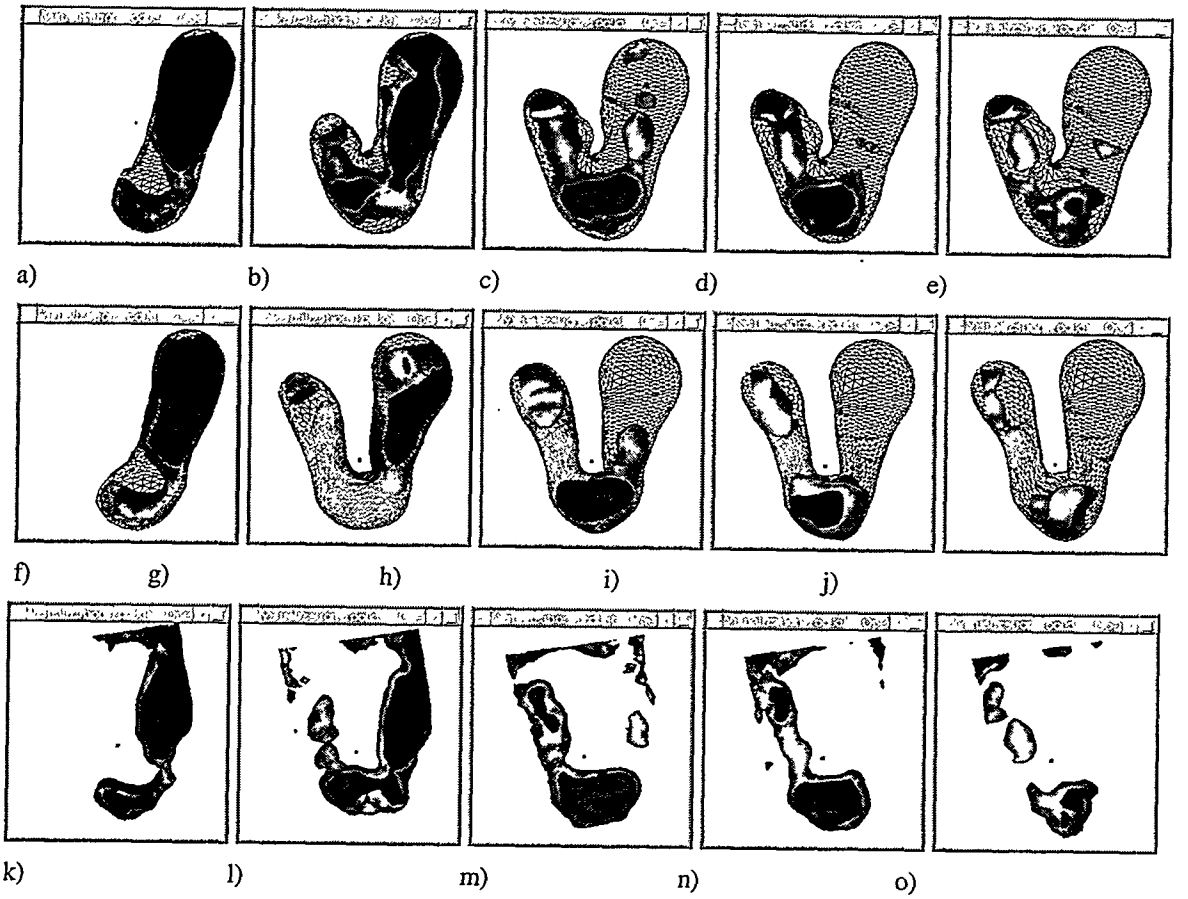

Figure 6. MAP estimates of surface (wireframe) and volume (isocontours at 0.425, 0.85 and 1.2) with α=3.16, β=0.56 for frames a) 46, b) 56, c) 66, d) 76 and e) 86; and with α=0.5, β=2.0 for frames f) 46, g) 56, h) 66, i) 76 and j) 86. 5 iterations of ML-EM for frames k) 46, l) 56, m) 66, n) 76 and o) 86.

A sphere was specified that is intended to contain the ventricle at all times and also to separate the ventricle from the inlet and outlet tubes. The intersection of the surface model with the sphere yields an estimate for the ventricular volume. Unfortunately, for the reconstruction in Fig 6a-e, the minimum volume and ejection fraction produced by this method have large errors (min vol ~250cc and ejection fraction ~13%; whereas the true values are 120cc and 40%, respectively). For the reconstruction in Figure 6f-j, lesser errors are observed (min vol ~ 129 cc and ejection fraction ~20%). Obviously, the surface is not a good estimator of the ventricular wall everywhere, for either the strong or weak surface models. On the other hand, if the volumetric reconstructions in Figure 6a-e and f-j are segmented by 1) applying the spherical region of interest discussed above, and 2) applying a threshold, above which voxels are counted as part of the ventricle and below which they are not (in the same way that one might process the ML-EM reconstructions), then excellent estimates of both the minimum ventricular volume and ejection fraction (min vol ~119 cc and ejection fraction ~37%) are obtained for the reconstructions in Figure 6a-e using a threshold of 0.425 (Figure 7a). These results are better than what one obtains with 5 iterations of ML-EM (Figure 7) with any value of threshold (Figure 7b). A histogram of estimated voxel intensities in the region specified by the sphere indicates a factor of at least 50% in tracer inhomogeneity (Figure 8).

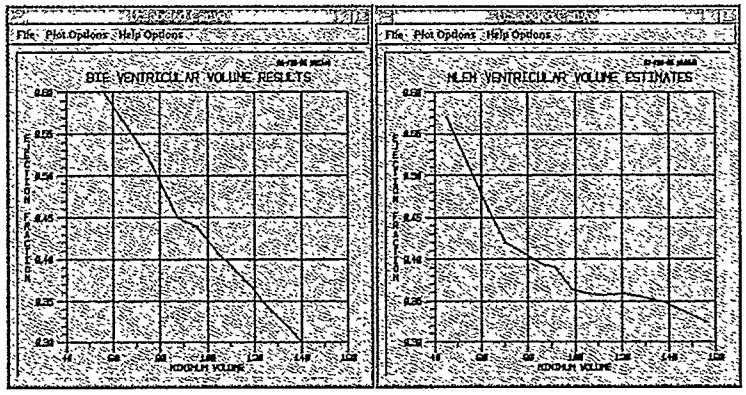

a) b)

Figure 7. Ejection fraction is plotted vs. minimum volume parameterized by the threshold used to determine if a voxel belongs to the ventricular volume or not for a) BIE (α=3.16, β=0.56) and b) 5 iterations of ML-EM. The circle indicates the correct answer (ejection fraction = 0.4 and minimum volume = 120cc).

Since the estimate of the surface does not appear to coincide well with the ventricular wall in all places (as evidenced by the poor estimates of ejection fraction using the surface model alone), one would not expect that wall motion can be extracted using our approach. However, in regions where the surface estimate coincides with the 0.425 intensity threshold, one might expect that the surface is in good agreement with ventricular wall location. There is a significant region of reconstruction 6a-e where this is true, namely where the diaphragm is located for the artificial heart (Figure 9b-c). We show in Figure 9a that our estimate of maximum wall motion in this area is about 5 mm. Unfortunately, at the time of writing, we did not know what the true wall motion was for this experiment, and so we can't comment on the quantitative accuracy of the BIE reconstructions in this regard.

5. CONCLUSIONS

We have extended our analysis of low-count, first-pass cardiac SPECT data in a Bayesian framework using deformable geometric models that admit smooth intensity variations within a bounding surface, across which rapid transitions in intensity can occur. In particular, the model assumes that the radiotracer distribution within the tubes and ventricle is smoothly distributed inside a volume defined by a patched Bezier surface. Prior distributions on the spatial variation of intensity and smoothness of the Bezier surface are used to penalize high-frequency solutions for both the surface and intensity, except in the tube/ventricle join region. In this region, where one expects high surface curvature, the surface prior is deweighted in a spherical region of diameter 5 cm with a user-defined center, to allow "kinks" to form at the joins. We jointly estimate the intensities of the voxels within the bounding surface as well as the positions of the control points of the surface from the raw data automatically for 41 consecutive frames of data, starting with simple initial configurations of the model for the first time frame. The introduction of surface kinks and use of Bezier patched surfaces were critical for allowing the process to be fully automated. The optimization process takes, on a DEC Alpha 500/500 (500 MB memory, 500 MHz processor), ~4 minutes per frame using a BFGS optimization algorithm.

The results show that the significant level of tracer inhomogeneity, observed and quantified in earlier work, prevent us from using the MAP estimate of the surface as a good estimate of the ventricular wall in all locations. On the other hand, the surface model appears to add value to the volumetric reconstruction problem, as we were able to identify a threshold that yields the correct volume of the ventricle before and after expansion (and hence the right ejection fraction) to within a few percent. This is in contrast to the case for 5 iterations of ML-EM, where all thresholds yield significant errors on either the ejection fraction or minimum volume (or both). We argued that wall motion can be extracted in those locations where the surface estimate is coincident with voxels at the threshold intensity, and produced an estimate of 5 mm for the wall motion in the experiment that produced the data we analyzed in this article.

There are still a few improvements that one could make to the analysis of this type of data that we haven't yet explored. First, since the activity level of the tracer is decaying in a predictable way, one should be able to determine how that decay will affect the optimal values of the hyperparameters as a function of time, and use those values. In the work reported here, the values for the hyperparameters that were determined to be optimal for the first analyzed frame were used for all subsequent frames, but since the decay rate indicates an activity level that changes by about a factor of 2 during the interesting frames, a more thorough approach may have an effect on the quality of the estimators at later frames. Second, the utility of incorporating hydrodynamic flow constraints on the time evolution of the 3D tracer distribution could possibly increase the quality of the results presented here. Our first attempts to determine the velocity distribution implied by our reconstructions of tracer intensity lead us to believe that this could be a fruitful area of effort, since the velocity distributions we have observed appear to be highly unphysical.

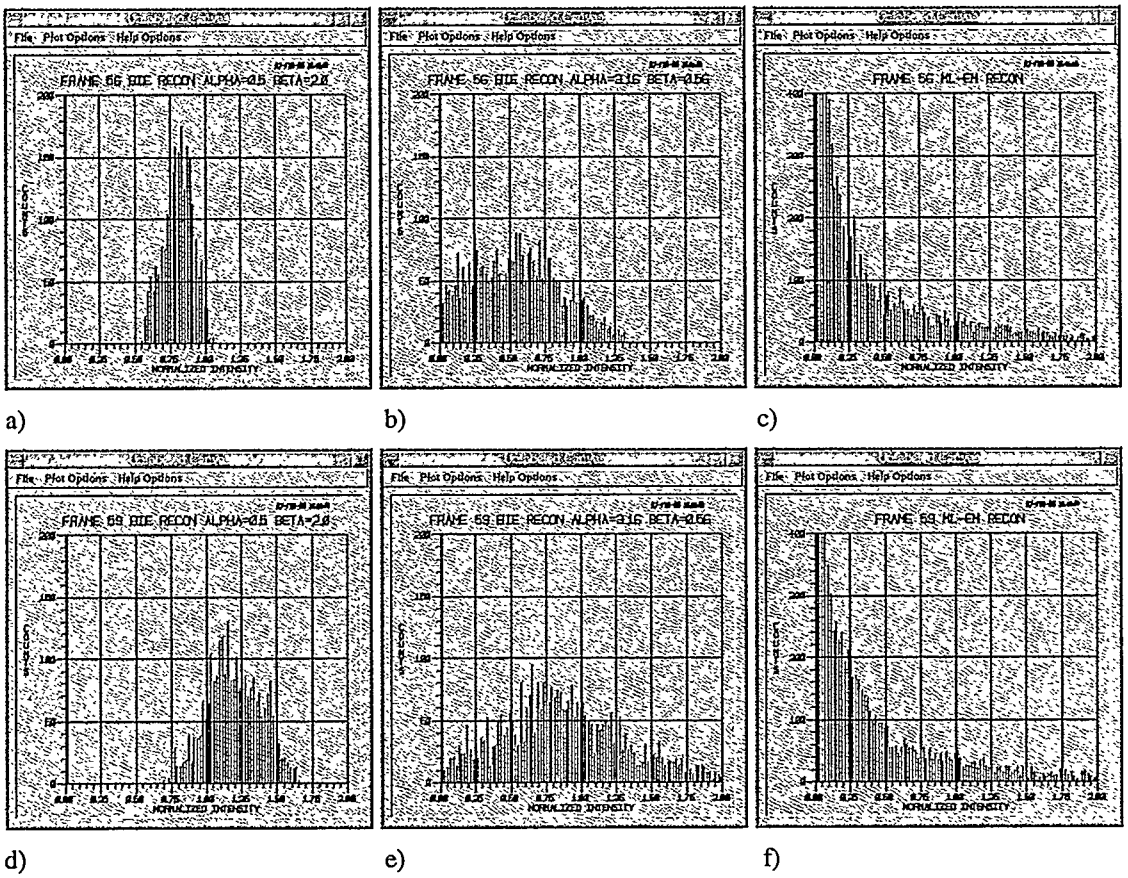

Figure 8. Histograms of estimated tracer intensities in ventricular region for frame 56 for a) BIE (with a=0.5, b= 2.0) b) BIE (with a=3.16, b=0.56) and c) 5 iterations of ML-EM. Similarly for frame 59 in d), e) and f). Partial voxel effects introduced by the surface model are removed for the BIE histograms.

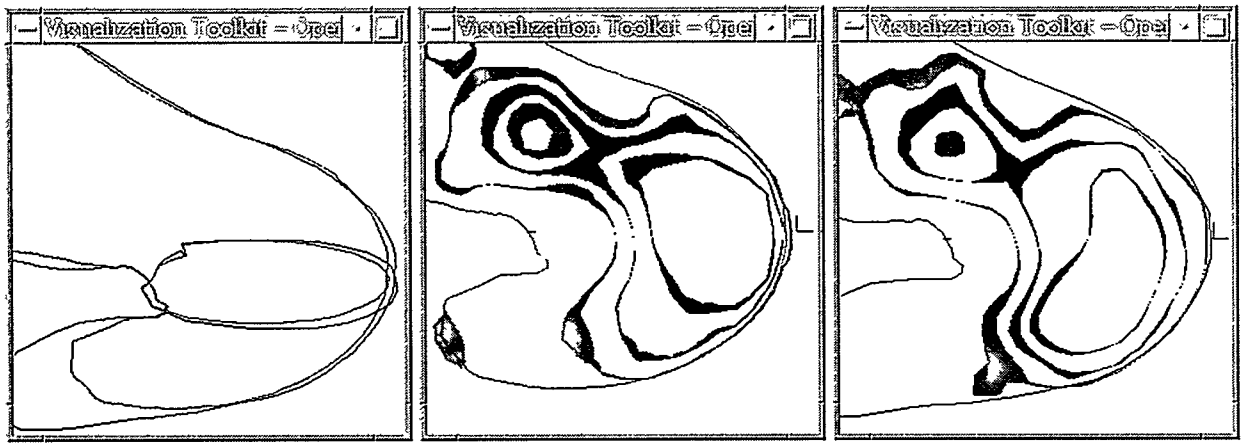

a) b) c)

Figure 9. Estimated motion of the diaphragm for the CardioWest artificial heart. The solid lines in a) are slices through the surface reconstructions for frames 58 and 59 (α=3.16, β=0.56). The movement of the surface estimate is ~5mm on the far right. The thin solid line in b) is a slice through the surface reconstruction for frame 58, while the 3 interior ribbons are 3 isocontours (at 0.425, 0.85 and 1.26) of the intensity reconstruction for frame 58; c) is the same as b) plotted for frame 59. The length of the axes plotted in b) and c) is 5 mm.

ACKNOWLEDGMENTS

This work was supported by the U.S. Department of Energy under contract 7405-ENG-36. We thank Irene Pang and Harry Barrett of the University of Arizona for supplying us with the FASTSPECT data and associated system matrix, complete with attenuation correction.

REFERENCES

1. W.P. Klein, H.H. Barrett, I. W. Pang, D.D. Patton, M.M. Rogulski, J.J. Sain, and W. Smith "FASTSPECT: Electrical and mechanical design of a high resolution dynamic SPECT imager," *Conference Record of the 1995 IEEE Nucl. Sci. Symp. & Med. Imaging Conf.* (IEEE, Los Alamitos, 1996), Vol. 2, pp. 931-933.
2. G.S. Cunningham and K.M. Hanson, "Uncertainty estimation for Bayesian reconstructions from low-count SPECT data," *Conference Record of the 1996 IEEE Nucl. Sci. Symp. & Med. Imaging Conf.* Available from Los Alamos National Laboratory as report number LAUR-96-4073.
3. G.S. Cunningham, K.M. Hanson, and X.L. Battle, "Three-dimensional reconstructions from low-count SPECT data using deformable models," *Optics Express* **2**, no. 6, pp. 227-236, 1998. Online at http://epubs.osa.org/opticsexpress.
4. G.S. Cunningham, A. Lehovich, and K.M. Hanson, "Bayesian estimation of regularization parameters for deformable surface models," *Proc. SPIE* (SPIE, Bellingham, 1996), Vol. 3661, pp. 562-573.
5. K.M. Hanson, R.L. Bilisoly, and G.S. Cunningham, "Kinky tomographic reconstruction," *Proc. SPIE* (SPIE, Bellingham, 1996), Vol. 2710, pp. 156-166.
6. X.L. Battle, G.S. Cunningham, and K.M. Hanson, "Tomographic reconstruction using 3D deformable models," *Phys. Med. Biol* **43**, pp. 983-990, 1998.
7. X.L. Battle, G.S. Cunningham, and K.M. Hanson, "3D tomographic reconstruction using geometrical models," *Proc. SPIE* (SPIE, Bellingham, 1997), Vol. 3034, pp. 346-357.
8. G. Farin, *Curves and Surfaces for CAGD: a practical guide,* 3rd edition, chapter 18, Academic Press, San Diego, 1993.
9. K.M. Hanson and G.S. Cunningham, "A computational approach to Bayesian inference," M.M. Meyer and J.L. Rosenberger, eds., *Computing Science and Statistics* (Interface Foundation, Fairfax Station, VA 22039-7460, 1996, Vol. 27, pp. 202-211.